Neuropharmacology 240 (2023) 109712

Contents lists available at ScienceDirect

Neuropharmacology

journal homepage: www.elsevier.com/locate/neuropharm

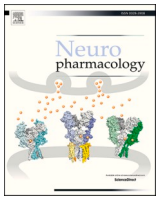

Selective inhibition of cannabinoid CB_1 receptor-evoked signalling by the interacting protein GAP43

Irene B. Maroto [a,b,c], Estefanía Moreno [d], Carlos Costas-Insua [a,b,c], Javier Merino-Gracia [a], Rebeca Diez-Alarcia [e,f,g], Alicia Álvaro-Blázquez [a,c], Ángeles Canales [h], Enric I. Canela [d], Vicent Casadó [d], Leyre Urigüen [e,f,g], Ignacio Rodríguez-Crespo [a,b,c], Manuel Guzmán [a,b,c,*]

[a] Department of Biochemistry and Molecular Biology, Instituto Universitario de Investigación Neuroquímica (IUIN), Complutense University, 28040, Madrid, Spain
[b] Centro de Investigación Biomédica en Red de Enfermedades Neurodegenerativas (CIBERNED), Instituto de Salud Carlos III, 28029, Madrid, Spain
[c] Instituto Ramón y Cajal de Investigación Sanitaria (IRYCIS), 28034, Madrid, Spain
[d] Department of Biochemistry and Molecular Biomedicine, Faculty of Biology and Institute of Biomedicine of the University of Barcelona, University of Barcelona, 08028, Barcelona, Spain
[e] Department of Pharmacology, University of the Basque Country/Euskal Herriko Unibertsitatea, 48940, Leioa, Spain
[f] Centro de Investigación Biomédica en Red de Salud Mental (CIBERSAM), 28029, Madrid, Spain
[g] Biocruces Bizkaia Health Research Institute, 48903, Barakaldo, Bizkaia, Spain
[h] Department of Organic Chemistry, Instituto Universitario de Investigación Neuroquímica (IUIN), Complutense University, 28040, Madrid, Spain

ARTICLE INFO

Keywords:
Cell signalling
Cannabinoid CB_1 receptor
Growth-associated protein of 43 kDa
Rho-associated coiled-coil containing protein kinase

ABSTRACT

Cannabinoids exert pleiotropic effects on the brain by engaging the cannabinoid CB_1 receptor (CB_1R), a presynaptic metabotropic receptor that regulates key neuronal functions in a highly context-dependent manner. We have previously shown that CB_1R interacts with growth-associated protein of 43 kDa (GAP43) and that this interaction inhibits CB_1R function on hippocampal excitatory synaptic transmission, thereby impairing the therapeutic effect of cannabinoids on epileptic seizures *in vivo*. However, the underlying molecular features of this interaction remain unexplored. Here, we conducted mechanistic experiments on HEK293T cells co-expressing CB_1R and GAP43 and show that GAP43 modulates CB_1R signalling in a strikingly selective manner. Specifically, GAP43 did not affect the archetypical agonist-evoked (*i*) $CB_1R/G_{i/o}$ protein-coupled signalling pathways, such as cAMP/PKA and ERK, or (*ii*) CB_1R internalization and intracellular trafficking. In contrast, GAP43 blocked an alternative agonist-evoked CB_1R-mediated activation of the cytoskeleton-associated ROCK signalling pathway, which relied on the GAP43-mediated impairment of $CB_1R/G_{q/11}$ protein coupling. GAP43 also abrogated CB_1R-mediated ROCK activation in mouse hippocampal neurons, and this process led in turn to a blockade of cannabinoid-evoked neurite collapse. An NMR-based characterization of the CB_1R-GAP43 interaction supported that GAP43 binds directly and specifically through multiple amino acid stretches to the *C*-terminal domain of the receptor. Taken together, our findings unveil a CB_1R-$G_{q/11}$-ROCK signalling axis that is selectively impaired by GAP43 and may ultimately control neurite outgrowth.

1. Introduction

The psychoactive components from the hemp plant *Cannabis sativa*, exemplified by Δ^9-tetrahydrocannabinol, and their endogenous analogues, the so-called endocannabinoids, bind to and activate the CB_1 and CB_2 cannabinoid receptors (CB_1R and CB_2R, respectively), which are members of the seven transmembrane G protein-coupled receptor (GPCR) superfamily (Pertwee et al., 2010; Piomelli, 2003). CB_1R is one of the most abundant GPCRs in the mammalian central nervous system, where it regulates a plethora of neurobiological functions, including learning and memory, emotions, feeding and motor behaviour (Katona and Freund, 2008), as well as brain development (Maccarrone et al., 2014). These diverse CB_1R-modulated processes rely on a complex array of receptor-evoked signal transduction events (Pertwee et al., 2010). Canonically, CB_1R couples to heterotrimeric $G_{i/o}$ proteins, thus inhibiting adenylyl cyclase (AC), decreasing cAMP levels and reducing protein

* Corresponding author. Department of Biochemistry and Molecular Biology, Instituto Universitario de Investigación Neuroquímica (IUIN), Complutense University, Madrid, 28040, Spain.
E-mail address: mguzman@quim.ucm.es (M. Guzmán).

https://doi.org/10.1016/j.neuropharm.2023.109712
Received 24 July 2023; Received in revised form 5 September 2023; Accepted 6 September 2023
Available online 7 September 2023
0028-3908/© 2023 The Authors. Published by Elsevier Ltd. This is an open access article under the CC BY-NC license (http://creativecommons.org/licenses/by-nc/4.0/).

kinase A (PKA) activation (Pertwee et al., 2010; Howlett et al., 1986). CB_1R also activates mitogen-activated protein kinase (MAPK) superfamily members, including extracellular signal-regulated kinase 1/2 (ERK1/2), with the concerted regulation of downstream transcription factors and gene expression. Other intracellular signalling platforms controlled by CB_1R include voltage-gated calcium channels and G protein-coupled inwardly-rectifying potassium channels, phospholipases C and A_2, and small GTPases such as Ras homolog gene family member A (RhoA) and Ras-associated protein 1 (Rap1) (Pertwee et al., 2010; Howlett and Abood, 2017; Nogueras-Ortiz and Yudowski, 2016).

CB_1R-evoked signalling is highly pleiotropic and relies largely on specific temporal and spatial contextual constraints. Ligand-biased agonism has been widely reported for CB_1R, and different G proteins can be recruited by the receptor in a ligand and cell type-dependent manner (Nogueras-Ortiz and Yudowski, 2016; Diez-Alarcia et al., 2016; Leo and Abood, 2021). Differential cell signalling pathways may also be triggered by the interaction of CB_1R with other membrane receptors, such as the adenosine A_2 receptor, as well as with specific cytoplasmic proteins, such as cannabinoid receptor-interacting protein 1a (Oyagawa and Grimsey, 2021; Oliver et al., 2020). To date, however, most of the studies on these putative protein-protein heterocomplexes had provided only subtle effects *in vivo*. Very recently, we have reported that growth-associated protein of 43 kDa (GAP43; also termed neuromodulin), a cytoskeleton-associated, membrane-bound protein highly abundant in excitatory pre-synapses, is a physiologically relevant CB_1R-interacting protein (Maroto et al., 2023). Using mass-spectrometry proteomic analysis and different *in vitro* and *in vivo* approaches, we showed that the *C*-terminal, intracellular domain of CB_1R interacts specifically with phosphorylated (active) GAP43 at a unique residue (S41), and that this interaction strongly inhibits receptor function in particular glutamatergic synapses of the mouse hippocampus, thus impairing one of the most prominent therapeutic effects of cannabinoids, namely their anti-convulsant activity (Maroto et al., 2023). However, that original report on the CB_1R-GAP43 interaction lacked an insight of the cell-signalling consequences and molecular patterns of the protein-protein association. Hence, the present study was undertaken to examine the cell-signalling consequences of the GAP43-mediated inhibition of CB_1R. We unveil that GAP43 does not affect canonical $CB_1R/G_{i/o}$ protein-coupled signalling but selectively impairs an atypical CB_1R-$G_{q/11}$ protein-Rho-associated coiled-coil containing protein kinase (ROCK) signalling axis, which may ultimately control neurite outgrowth. We also provide an NMR-based characterization of the amino acid stretches of GAP43 that preferentially interact with CB_1R. Taken together, these findings may contribute to understanding the contextual factors that control the promiscuous CB_1R-evoked signalling in the brain and may shed light on the molecular determinants that drive the anti-convulsant activity of cannabinoids.

2. Materials and methods

2.1. Gene constructs

The pEGFP-C2 plasmid was purchased to ClonTech, and we generated pEGFP-hGAP43 by standard cloning procedures. The cDNA encoding hGAP43 was acquired from DNAsu (Clone ID HsCD00042260). The pcDNA3.1(+) plasmid was purchased from Invitrogen. pcDNA3.1-hCB_1R and pcDNA-hGAP43 were built by PCR and restriction cloning. The 3XFLAG-tagged version of pcDNA3.1-hCB_1R was obtained by using IVA cloning. All gene constructs were validated by Sanger sequencing before use (Maroto et al., 2023; Costas-Insua et al., 2021).

2.2. Cell culture, transfection and drug treatments

The human HEK293T cell line was purchased from the American Type Culture Collection (Manassas, VA, USA). Cells were grown in Dulbecco's modified Eagle's medium (DMEM) supplemented with 10% foetal bovine serum (FBS) (v/v), 1 mM sodium pyruvate, 2 mM L-glutamine and 1% streptomycin/penicillin. Cells were maintained at 37 °C in an atmosphere with 5% CO_2 and were periodically checked for the absence of mycoplasma contamination. Cells were transiently transfected with the corresponding cDNA plasmid using polyethylenimine (Sigma, Steinheim, Germany) in a 4:1 mass ratio to DNA, except for immunofluorescence experiments, in which Lipofectamine 2000 (Thermo Fisher Scientific) was used. For Western blot analysis, 48 h after transfection, cells were transferred to 6-well dishes, FBS-starved overnight, and treated for 5 min with vehicle (DMSO, 0.1% v/v final concentration) or WIN 55,212–2 (WIN; 100 nM, Sigma). For analysing PKA phosphorylated substrates, forskolin (0.5 μM, Tocris, Bristol, United Kingdom) or vehicle was added right after WIN/vehicle and maintained for an additional 10-min period. To block $G\alpha_{q/11}$ proteins, YM-254890 (1 μM; MedChem, NJ, USA) (or vehicle as control) was added to cells 30 min before WIN or vehicle (5-min further incubation). Cells were washed in ice-cold PBS and directly frozen for further analyses. For immunofluorescence, 12-μm diameter coverslips were coated with 0.1 mg/ml poly-D-Lysine for 1 h at 37 °C. Cells were seeded on the coverslips at a density of 25,000 cells/cm^2 and transfected with the corresponding plasmid. Forty-eight h after transfection, cells were serum-starved overnight, treated, and fixed in paraformaldehyde solution (PFA; 4% in PBS) during 15 min at room temperature. Every condition was assayed in triplicate within each individual experiment.

Primary hippocampal neurons were obtained from 0-2-day old C57BL/6N mice of mixed sexes. The experimental procedures were performed in accordance with the guidelines and approval of the Animal Welfare Committees of Universidad Complutense de Madrid and Comunidad de Madrid, and the directives of the Spanish Government and the European Commission. Dissection was followed by mechanical disaggregation and a papain dissociation procedure (Worthington, Columbus, OH, USA). Cells were nucleofected with 3 μg of the aforementioned pcDNA3.1 empty plasmid or pcDNA3.1-hGAP43 plasmid using the Amaxa mouse neuron Nucleofector kit (Lonza, Basel, Switzerland). Cells were seeded on plates precoated with 0.1 mg/ml poly-D-Lysine and 3 μg/ml laminin at a density of 200,000 cells/cm^2 in Neurobasal medium supplemented with 10% FBS (v/v), 1 mM sodium pyruvate, 0.5 mM L-glutamine and 1% streptomycin/penicillin. Three hours later, FBS was substituted with B27 supplement (Blázquez et al., 2011). This media was renewed every two days adding cytosine arabinoside (10 μM; Sigma, Steinheim, Germany) to block glial cell growth. At 7 days *in vitro* (DIV), neurons were treated with WIN or vehicle for 5 min and then fixed or frozen for immunofluorescence or Western blot assays, respectively. Every condition was assayed in triplicate within each individual experiment.

2.3. Western blot

As previously described (Maroto et al., 2023; Costas-Insua et al., 2021), snap-frozen HEK293T cells or primary cultured neurons were homogenized and lysed for protein extraction in ice-cold lysis buffer containing 50 mM Tris, 0.1% Triton X-100, 1 mM EDTA, 1 mM EGTA, 50 mM NaF, 10 mM sodium β-glycerophosphate, 5 mM sodium pyrophosphate and 1 mM sodium orthovanadate (pH 7.5), supplemented with 0.1 mM phenylmethane-sulphonylfluoride, 0.1% β-mercaptoethanol and 1 μM microcystin. Samples were cleared by centrifugation at 12, 000*g* for 15 min at 4 °C, and the supernatants were collected. Protein concentration was determined by the Bradford method. Then, 20-30-μg aliquots of total protein were mixed with 5X SDS sample buffer and boiled at 95 °C for 5 min (except for CB_1R detection, whose samples were heated at 55 °C for 10 min). Equal amounts of protein samples were resolved on 12% SDS–PAGE, and subsequently transferred to polyvinylidene difluoride (PVDF) membranes (Bio-Rad, Madrid, Spain). After incubation for at least 1 h in blocking buffer containing 5% w/v bovine serum albumin (BSA) in Tris buffered saline-0.1% Tween 20

(TBS-T), membranes were blotted overnight at 4 °C with the following primary antibodies and dilutions: rabbit anti-PKA phospho-substrates (1:1000, CST, #9621), rabbit anti-phospho-ROCK2 (1:750, Gene Tex, #GTX122651), mouse anti-ROCK2 (1:750, SCB, #sc-398519), rabbit anti-phospho-cofilin (1:1000, CST, #3313), mouse anti-cofilin (1:1000, SCB, #sc-376476), rabbit anti-phospho-ERK1/2 (1:1000, CST, #9101), mouse anti-ERK1/2 (1:1000, CST, #4696), mouse anti-α-tubulin (1:10, 000, Sigma-Aldrich, #T9026), mouse anti-*pan*-GAP-43 (clone 7B10; 1:1000, Santa Cruz Biotechnology, #sc-33705), mouse anti-FLAG M2 (1:1000, Sigma-Aldrich, #F3165), mouse anti-GFP (1:1000, Thermo Fisher Scientific, #MA5-15 256). PVDF membranes were then rinsed 3 times with TBS-T and incubated with the corresponding mouse or rabbit secondary antibodies (mouse IgG HRP-linked antibody, 1:5000, Sigma-Aldrich, #NA-931-1; rabbit IgG HRP-linked antibody, 1:5000, Sigma-Aldrich, #NA-934V) coupled to horseradish peroxidase for 1.5 h at room temperature. After washing 3 times for 10 min with TBS-T, membranes were developed using an enhanced chemiluminescence kit (Bio-Rad, Madrid, Spain). Densitometric analysis of the relative expression of the protein of interest *versus* the corresponding loading control was performed with FIJI ImageJ opensource software (NIH, Bethesda, MD). Western blot images were cropped for clarity. Electrophoretic migration of molecular weight markers is depicted on the left-hand side of each blot. Full-length, uncropped blots are shown in Suppl. Fig. 1.

2.4. Determination of cAMP concentration

Homogeneous time-resolved fluorescence (HTRF) energy transfer assays were performed using the Lance Ultra cAMP kit (PerkinElmer) as previously reported (Costas-Insua et al., 2021; Moreno et al., 2014). HEK293T cells (1000 per well) were seeded in medium containing 50 μM zardeverine in white ProxiPlate 384-well microplates (PerkinElmer) at 25 °C and stimulated with 100 nM WIN or vehicle for 15 min before adding 0.5 μM forskolin or vehicle, which were kept for an additional 15-min period. Fluorescence at 665 nm was analysed on a PHERAstar Flagship microplate reader equipped with an HTRF optical module (BMG Lab technologies, Offenburg, Germany). cAMP values from basal stimulation in the absence of forskolin or agonists were subtracted from cAMP values obtained in each condition. cAMP values are expressed as the percentage of the forskolin-treated cells in each condition. Every condition was assayed in triplicate within each individual experiment.

2.5. Antibody-capture [^{35}S]GTPγS scintillation proximity assay

To obtain the membrane fraction, HEK293T cell pellets (approximately 500-mg weight) were homogenized in 50 mM Tris-HCl, 1 mM EGTA, 3 mM $MgCl_2$ and 1 mM DTT, pH 7.4, supplemented with 250 mM sucrose, and centrifuged at 1000*g* for 15 min at 4 °C. Supernatants were recovered and centrifuged at 40,000*g* for 10 min at 4 °C. The pellets obtained were resuspended in 10 vol of homogenization buffer and recentrifuged at 40,000*g* for 10 min at 4 °C. The homogenates were centrifuged twice at 1,100*g* and at 40,000*g* for 10 min at 4 °C. The resultant pellets were resuspended in fresh cold centrifugation buffer (50 mM Tris-HCl, 1 mM EGTA, 3 mM $MgCl_2$ and 1 mM DTT, pH 7.4) and centrifuged. Protein content was determined by the Bradford method. Specific activation of different subtypes of Gα protein subunits was determined using a homogeneous protocol of [^{35}S]GTPγS scintillation proximity assay coupled to the use of the following anti-Gα antibodies: mouse monoclonal anti-$G\alpha_{i1}$ (1:20, SCB, #sc-56536), mouse monoclonal anti-$G\alpha_o$ (1:40, SCB, #sc-393874), mouse monoclonal anti-$G\alpha_{q/11}$ (1:20, SCB, #sc-515689), rabbit polyclonal anti-$G\alpha_s$ (1:20, SCB, #sc-377435) and rabbit polyclonal anti-$G\alpha_z$ (1:60, Antibodies on-line #ABIN653561), as previously described (Diez-Alarcia et al., 2016; Costas-Insua et al., 2021). [^{35}S]GTPγS binding was performed in 96-well Isoplates (PerkinElmer Life Sciences, Maanstraat, Germany) with 200 μl of buffer (1 mM EGTA, 3 mM $MgCl_2$, 100 mM NaCl, 0.2 mM DTT, 50 mM Tris–HCl, pH 7.4), 0.4 nM [^{35}S]GTPγS, 10 μg of protein per well, and different concentrations of GDP depending on the Gα subunit subtype tested. After a 2-h incubation period at 30 °C, 20 μl of Igepal 1% + SDS 0.1% was added to each well, and plates were incubated at 22 °C for 30 min with gentle agitation. Then, the specific antibody for the Gα subunit was added to each well before an additional 90-min incubation period at room temperature. Polyvinyltoluene SPA beads coated with protein A (PerkinElmer, Madrid, Spain) were then added (0.75 mg of beads per well), and plates were incubated for 3 h at room temperature with gentle agitation. Finally, plates were centrifuged (5 min at 1000*g*), and bound radioactivity was detected on a MicroBeta TriLux scintillation counter (PerkinElmer, Madrid, Spain). To test their effect on the [^{35}S]GTPγS binding to the different Gα subunit subtypes in the different experimental conditions, a single submaximal concentration (10 μM) of WIN was tested. Nonspecific binding was defined as the remaining [^{35}S]GTPγS binding in the presence of 10 μM unlabelled GTPγS. Specific [^{35}S]GTPγS binding values were transformed to the percentage of basal [^{35}S]GTPγS binding (in the absence of any exogenous drug) obtained for each Gα protein. Every condition was assayed in triplicate within each individual experiment.

2.6. Dynamic mass redistribution (DMR)

The overall cell signalling signature was determined using an EnSpire® Multimode Plate Reader (PerkinElmer, Waltham, MA, USA) by a label-free technology. Refractive waveguide grating optical biosensors, integrated in 384-well microplates, allow extremely sensitive measurements of changes in local optical density in a detecting zone up to 150 nm above the surface of the sensor. Cellular mass movements induced upon receptor activation were detected by illuminating the underside of the biosensor with polychromatic light and measured as changes in wavelength (in pm) of the reflected monochromatic light, which is a sensitive function of the index of refraction. The magnitude of this wavelength shift is directly proportional to the amount of DMR. Briefly, 24 h before the assay, HEK293T cells expressing FLAG-CB_1R were seeded at a density of 10,000 cells per well in 384-well sensor microplates with 30 μl growth medium and cultured for 24 h (37 °C, 5% CO_2) to obtain 70–80% confluent monolayers. Prior to the assay, cells were preincubated for 30 min with vehicle, Y-27632 (10 μM; MedChem, NJ, USA) or YM-254890 (1 μM). Then, cells were washed twice with assay buffer (HBSS with 20 mM HEPES, pH 7.15) and incubated for 2 h in 30 μl of assay-buffer per well with 0.1% DMSO in the reader at 24 °C. Hereafter, the sensor plate was scanned, and a baseline optical signature was recorded before adding 10 μl of WIN at 100 nM dissolved in assay buffer containing 0.1% DMSO. Then, the resulting shifts of reflected light wavelength (pm) or DMR responses were monitored for at least 2000 s. Kinetic results were analysed using EnSpire Workstation Software v 4.10.

2.7. Immunofluorescence and receptor internalization assays

For immunofluorescence, as previously reported (Maroto et al., 2023), fixed cultured cells were permeabilized and blocked in PBS containing 0.25% Triton X-100 (Sigma) and 5% goat serum (Pierce Biotechnology, Rockford, IL, USA) for 1 h at room temperature. Primary antibodies were diluted directly into the blocking buffer and coverslips were incubated overnight at 4 °C with the following primary antibodies: rabbit anti-EEA1 antibody (1:100, CST, #2411), mouse anti-FLAG M2 antibody (1:1000, Sigma-Aldrich, #F3165), rabbit anti-LAMP1 antibody (1:750, Abcam, Ab24170), mouse anti-*pan*-GAP43 (1:1000, SCB, #sc-33705), guinea pig anti-CB_1R (1:500, Frontier Institute, #CB1-GP-Af530), rabbit anti-βIII-tubulin (1:500, BioLegend, #802001), mouse anti-βIII-tubulin (1:500, Chemicon, #MAB1637), rabbit anti-phospho-ROCK2 (1:500, Gene Tex, #GTX122651). After 3 washes with PBS plus 0.25% Triton X-100 for 10 min, samples were subsequently incubated for 2 h at room temperature with the appropriate

cross-adsorbed AlexaFluor 488 goat anti-mouse IgG (Invitrogen, #A-28175), AlexaFluor 488 goat anti-rabbit IgG (Invitrogen, #A-11008), AlexaFluor 546 goat anti-mouse IgG (Invitrogen, #A-11030), AlexaFluor 546 goat anti-rabbit IgG (#A-11035), AlexaFluor 647 goat anti-mouse IgG (1:1000, Invitrogen, #A-21235), AlexaFluor 647 goat anti-guinea pig IgG (Invitrogen, #A-21450) at 1:500 or 1:1000 depending on the dilution of the primary antibody, and the nuclear marker 4',6-diamidino-2-phenylindole (DAPI) (1:10,000) to visualize nuclei (all from Invitrogen, Carlsbad, CA, USA) diluted in blocking buffer. After washing 3X in PBS 0.25% Triton X-100 for 10 min, coverslips cell-side down were mounted onto microscope slides using Mowiol® mounting media.

The protocol for quantification of receptor internalization in HEK293T cells expressing FLAG-CB_1R was described in (Zhuang and Matsunami, 2008). Briefly, for live-cell immunofluorescence, cells seeded on coverslips were transferred from their culture dishes to a new 150-mm dish cell-side up and placed on ice. Mouse anti-FLAG M2 antibody (1:1000, Sigma-Aldrich, #F3165) diluted in a staining solution containing Minimum Essential Media (MEM) with 10 mM HEPES, supplemented with 15 mM NaN_3 to minimize receptor endocytosis during sample handling (Zhuang and Matsunami, 2008). One hundred μl of the solution was applied per coverslip and incubated on ice for 1 h. At the end of the incubation, the cover glasses were carefully transferred back to its original 150-mm dish and washed three times with cold washing solution for live-cell immunocytochemistry composed of Hank's Balanced Salt Solution (HBSS) with 10 mM HEPES and 15 mM NaN_3. The corresponding secondary antibody AlexaFluor 647 goat anti-mouse IgG (1:1000, Invitrogen, #A-21235) was diluted as well in staining solution and incubated for 30 min on ice. Afterwards, coverslips were washed again three times. Finally, the washing solution was replaced with 4% PFA for 15 min to fix the cells. A subsequent immunostaining step was performed as described above. Cells were permeabilized with PBS containing 0.25% Triton X-100 and 5% goat serum for 1 h. Rabbit anti-CB_1R primary antibody (1:500, Frontier Institute, #CB1-Rb-Af380), raised against the *C*-terminal domain of CB_1R, and AlexaFluor 546 goat anti-rabbit IgG (1:1000, Invitrogen, #A-11035) as secondary antibody were used. Every condition was assayed in triplicate within each individual experiment.

Confocal fluorescence images were acquired by using LAS-X software version 3.4.2.18368 with a SP8 confocal microscope (Leica Microsystems, Mannheim, Germany). All quantifications were obtained from a minimum of 3 fields per condition. Immunoreactive positive area was measured using FIJI ImageJ open-source software establishing a threshold to measure only specific signal. For colocalization assays, the resulting binary mask was then used along the built-in measure function to acquire the total immunoreactive area among all the pixels inside the binary mask overlaid on top of the original image. The obtained value was then normalized to the number of DAPI-positive cell nuclei. Data were then expressed as normalized to control. In primary neuron cultures, neurite length was measured systematically in 4 fields of 1 mm^2 per condition (in triplicate) using the free Image J plugin NeuronJ, and the mean value (in mm) was normalized to the control condition (in triplicate). None of the secondary antibodies produced any signal in preparations incubated in the absence of the corresponding primary antibodies. Representative images for each condition were prepared for figure presentation by applying brightness and contrast adjustments uniformly.

2.8. Nuclear magnetic resonance (NMR)

GAP43 was produced recombinantly in a bacterial expression system with pBH4 plasmid encoding 6xHis-tagged hGAP43 following standard immobilized-metal affinity chromatography (IMAC) purification. For the NMR experiments, GAP43 was expressed in minimal M9 medium, supplemented with ^{15}N-NH_4-Cl and purified likewise (Maroto et al., 2023). NMR spectra were acquired using a Bruker 700 MHz spectrometer equipped with 5 mm triple channel inverse (TCI) cryoprobe for $^{1}H/^{13}C/^{15}N/^{2}D$ with Z gradient coil. Spectra were analysed using TopsSpin version 3.5 and CcpNmr Analysis 3.0 (Skinner et al., 2016; Mureddu et al., 2020). ^{1}H-^{15}N heteronuclear single quantum coherence (HSQC)-based titrations were performed using ^{15}N-labelled GAP43 in 20 mM phosphate buffer (pH 6.0) with 40 mM NaCl and 10% D_2O at 298 K. HSQC resonances were identified based on repository-deposited assignments (Biological Magnetic Resonance Bank code 19246 (Flamm et al., 2016) https://bmrb.io/data_library/summary/index.php?bmrbId=19246). Peaks were transferred to the most likely nearest neighbour using the software CCPN (Mureddu et al., 2020). Ambiguities were omitted from the analysis. Chemical shift perturbations caused by the interaction of GAP43 with an unlabelled hCB_1R *C*-terminal peptide were calculated and mapped to the sequence to identify possible interacting domains. The hCB_1R peptide (sequence CLHKHANNAASVHRAAESSIKSTVKIAK; amino acids 431–458; C449 of wild-type CB_1R was replaced with S449 to reduce peptide reactivity) was synthesised by the Proteomics Unit of Madrid Complutense University.

2.9. Statistics

Data are presented as means ± SEM and the number of biological replicates is indicated in every case. Graph elaboration and statistical analysis were performed with GraphPad Prism version 8.0.1 (GraphPad Software, San Diego, CA, USA). All variables were first tested for normality (Kolmogorov–Smirnov's and Shapiro-Wilk's test) and homoscedasticity (Levene's test) before analysis. The particular statistical tests applied are indicated in each figure legend. We considered p-values <0.05 as statistically significant. The number of technical replicates is provided in the corresponding Material and Methods subsection.

3. Results

3.1. GAP43 does not affect CB_1R-$G\alpha_{i/o}$ protein-evoked signalling in HEK293T cells

We have previously shown that GAP43 interacts directly with CB_1R and inhibits receptor function at hippocampal excitatory synapses (Maroto et al., 2023). To identify the precise signalling cascades affected by this protein-protein interaction, we first evaluated the effect of GAP43 on the classical CB_1R-mediated inhibition of the cAMP pathway (Howlett et al., 1986). Thus, HEK293T cells expressing FLAG-tagged CB_1R were co-transfected with GFP-labelled GAP43 or a GFP control vector (Suppl. Fig. 2A). Then, cells were pretreated with vehicle or the synthetic CB_1R agonist WIN 55,212-2 (WIN; 100 nM, 15 min) and subsequently treated with vehicle or the AC activator forskolin (FSK; 0.5 μM, 15 min) to induce cAMP formation ($F_{(2, 12)} = 49.71$; FSK vs vehicle $p < 0.0001$, FSK + WIN vs FSK $p = 0.0023$). We observed that GAP43 expression did not affect the expected WIN-mediated reduction of FSK-induced cAMP concentration ($F_{(2, 12)} = 49.71$; FSK vs vehicle $p < 0.0001$, FSK + WIN vs FSK $p = 0.0037$; Fig. 1A). To further support this observation, we evaluated the levels of PKA phosphorylated substrates by Western blot and found that the expected WIN-mediated reduction of FSK-triggered PKA-substrates phosphorylation ($F_{(3, 24)} = 21.29$; FSK vs vehicle $p < 0.0001$, FSK + WIN vs FSK $p = 0.0002$) was not changed by GAP43 expression ($F_{(3, 24)} = 21.29$; FSK vs vehicle $p = 0.0088$, FSK + WIN vs FSK $p = 0.0004$; Fig. 1B).

Another classical $G\alpha_{i/o}$-mediated downstream effector of CB_1R is ERK1/2 (Pertwee et al., 2010). We therefore evaluated WIN-evoked ERK1/2 phosphorylation (activation) in HEK293T cells in the presence or absence of GAP43. WIN challenge (100 nM, 5 min) caused a remarkable increase in ERK1/2 phosphorylation in control conditions ($F_{(1, 16)} = 27.74$, WIN vs vehicle $p = 0.0046$) and once again, GAP43 expression did not affect agonist-evoked CB_1R action ($F_{(1, 16)} = 27.74$, WIN vs vehicle $p = 0.0174$; Fig. 1C). We next measured the coupling of

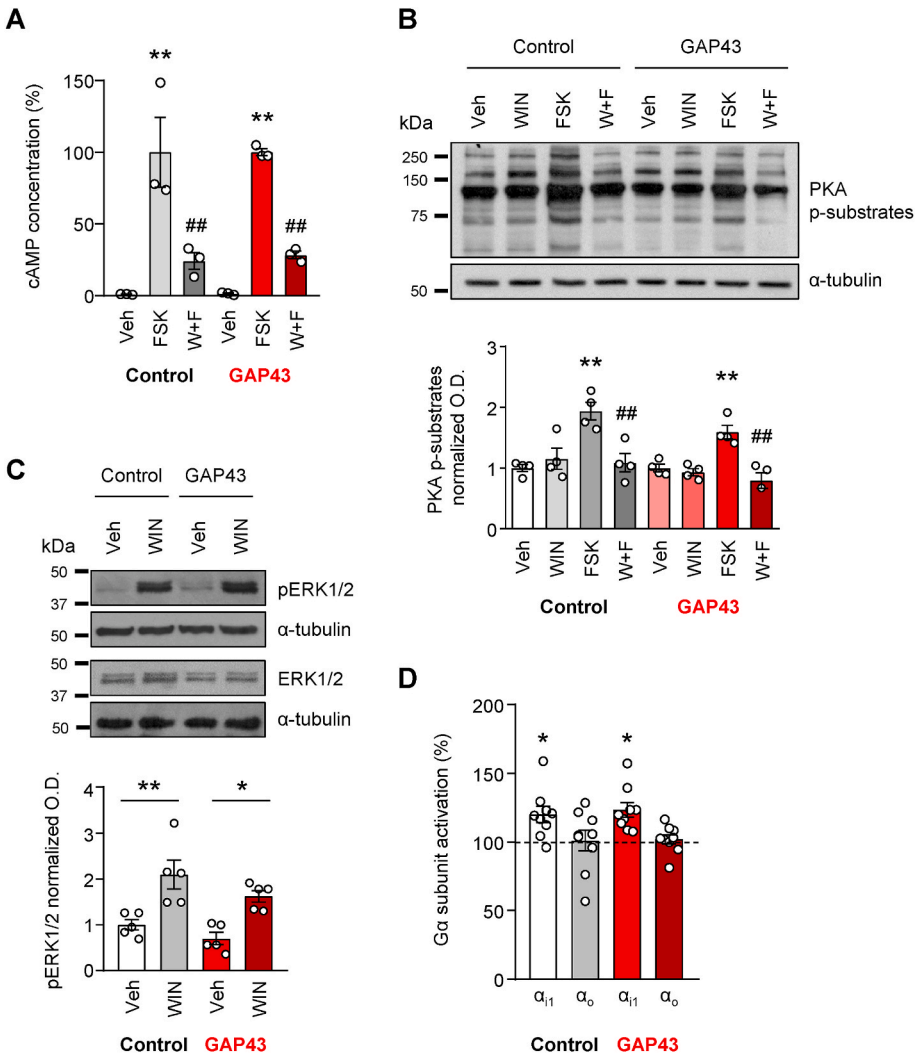

Fig. 1. GAP43 does not affect CB_1R-$G\alpha_{i/o}$ protein-evoked signaling in HEK293T cells. **A.** HEK293T cells transfected with CB_1R, and a control vector or a GAP43-encoding vector, were treated with vehicle or WIN (100 nM, 15 min) and subsequently with forskolin (FSK; 0.5 μM, 15 min) to determine cAMP concentration (means ± SEM, n = 3 experiments, **p < 0.01 from vehicle and ##p < 0.01 from FSK by two-way ANOVA with Tukey's multiple comparison test). **B.** HEK293T cells transfected with CB_1R, and a control vector or a GAP43-encoding vector, were treated with vehicle or WIN (100 nM, 5 min) and subsequently with FSK (0.5 μM, 10 min). Representative Western blots and quantification of optical density (O.D.) values of PKA phosphorylated substrates relative to those of the loading control are shown (means ± SEM, n = 4 experiments; **p < 0.01 from vehicle and ##p < 0.01 from FSK by two-way ANOVA with Tukey's multiple comparison test). **C.** HEK293T cells transfected with CB_1R, and a control vector or a GAP43-encoding vector, were treated with vehicle or WIN (100 nM, 5 min). Representative Western blots and quantification of optical density (O.D.) values of phosphorylated ERK1/2 relative to those of the loading control are shown (means ± SEM, n = 5 experiments; *p < 0.05, **p < 0.01 by two-way ANOVA with Tukey's multiple comparison test). **D.** [^{35}S]GTPγS scintillation proximity assays coupled to immunoprecipitation with specific antibodies against $G\alpha_{i1}$ and $G\alpha_o$ subunits were conducted in membrane homogenates from HEK293T cells transfected with CB_1R and a control vector or a GAP43-encoding vector. Data are shown as percentage of [^{35}S]GTPγS basal binding values obtained for each specific subunit upon WIN application (means ± SEM, n = 9 experiments, 100% indicated with a dashed line, *p < 0.05 from basal by one sample Student's t-test and n. s. from control by two-tailed unpaired Student's t-test).

CB_1R to $G\alpha_{i/o}$ proteins in the absence or presence of GAP43. We conducted [^{35}S]GTPγS scintillation proximity assays coupled to immunoprecipitation with specific antibodies raised against archetypical $G\alpha_{i/o}$ subunits. In HEK293T cells expressing only CB_1R, we observed a cannabinoid agonist-mediated activation of $G\alpha_{i1}$ protein ($t_{(8)} = 3.394$; p = 0.0094) but not of $G\alpha_o$ protein ($t_{(8)} = 0.1361$; p = 0.8951; Fig. 1D), as might be expected in this cell type (Anavi-Goffer et al., 2007; Burford et al., 1998). This activation of $G\alpha_{i1}$ was preserved in the presence of GAP43 ($G\alpha_{i1}$: $t_{(8)} = 4.404$; p = 0.0023; $G\alpha_o$: $t_{(8)} = 0.5823$; p = 0.5762; $G\alpha_{i1}$ control vs $G\alpha_{i1}$ GAP43 p = 0.6817, $G\alpha_o$ control vs $G\alpha_o$ GAP43 p = 0.9113; Fig. 1D).

Taken together, these data support that classical CB_1R-$G\alpha_{i/o}$ protein-coupled signalling pathways are not affected by GAP43.

3.2. GAP43 does not affect CB_1R internalization and recycling in HEK293T cells

GAP43 can control the internalization of plasma membrane receptors (Han et al., 2013). Hence, we next evaluated the effect of GAP43 expression on agonist-evoked CB_1R internalization. For this purpose, we used HEK293T cells expressing an *N*-terminally FLAG-tagged CB_1R, which allows immunolabelling cell-surface receptors and relating them, after membrane permeabilization, to total cell receptors as stained with an anti-CB_1R-*C*-terminal antibody. Cells were transfected with GAP43 fused to GFP or a GFP control vector and incubated with vehicle or WIN (100 nM, 10 or 40 min) (Fig. 2A). At the shorter incubation time of 10 min, WIN did not alter the levels of cell-surface CB_1Rs compared to vehicle, and this value was then taken as a reference to calculate the fold-change of WIN over vehicle for each time interval. At the longer incubation time of 40 min, WIN caused a similar ~50% receptor internalization in either control vector-transfected ($F_{(1, 20)} = 35.88$, p = 0.0056) or GAP43 vector-transfected cells ($F_{(1, 20)} = 35.88$, p = 0.0008; Fig. 2A), thus indicating that GAP43 does not impact CB_1R internalization.

Internalized CB_1R tends to be localized primarily in early endosomes (Fletcher-Jones et al., 2020). Accordingly, after WIN challenge for 10 min, we found a residual extent of internalization to early endosomes, as assessed by the colocalization of FLAG-CB_1R (facing the luminal side of the endocytosis vesicle) and the early endosome antigen 1 (EEA1) ($F_{(1, 20)} = 5.576$, WIN vs vehicle in control p = 0.6564, WIN vs vehicle in GAP43 p = 0.1639; Fig. 2B). In line with our aforementioned observations, CB_1R showed an increased localization to early endosomes upon a 40-min WIN exposure, that was similar for control vector-expressing and GAP43-expressing cells ($F_{(1, 20)} = 29.10$, WIN vs vehicle in control p = 0.0032, WIN vs vehicle in GAP43 p = 0.0095). From early endosomes, CB_1R can be recycled to the plasma membrane or targeted to lysosomes for degradation (Martini et al., 2007). After either 10 or 40-min WIN application, we found no change in the co-localization between FLAG-CB_1R and the lysosomal-associated membrane protein 1 (LAMP1) marker (at 10 min: $F_{(1, 8)} < 0.0001$, WIN vs vehicle in control p > 0. 9999, WIN vs vehicle in GAP43 p > 0. 9999; at 40 min: $F_{(1, 8)} = 0.0737$, WIN vs vehicle in control p > 0. 9999, WIN vs vehicle in GAP43 p =

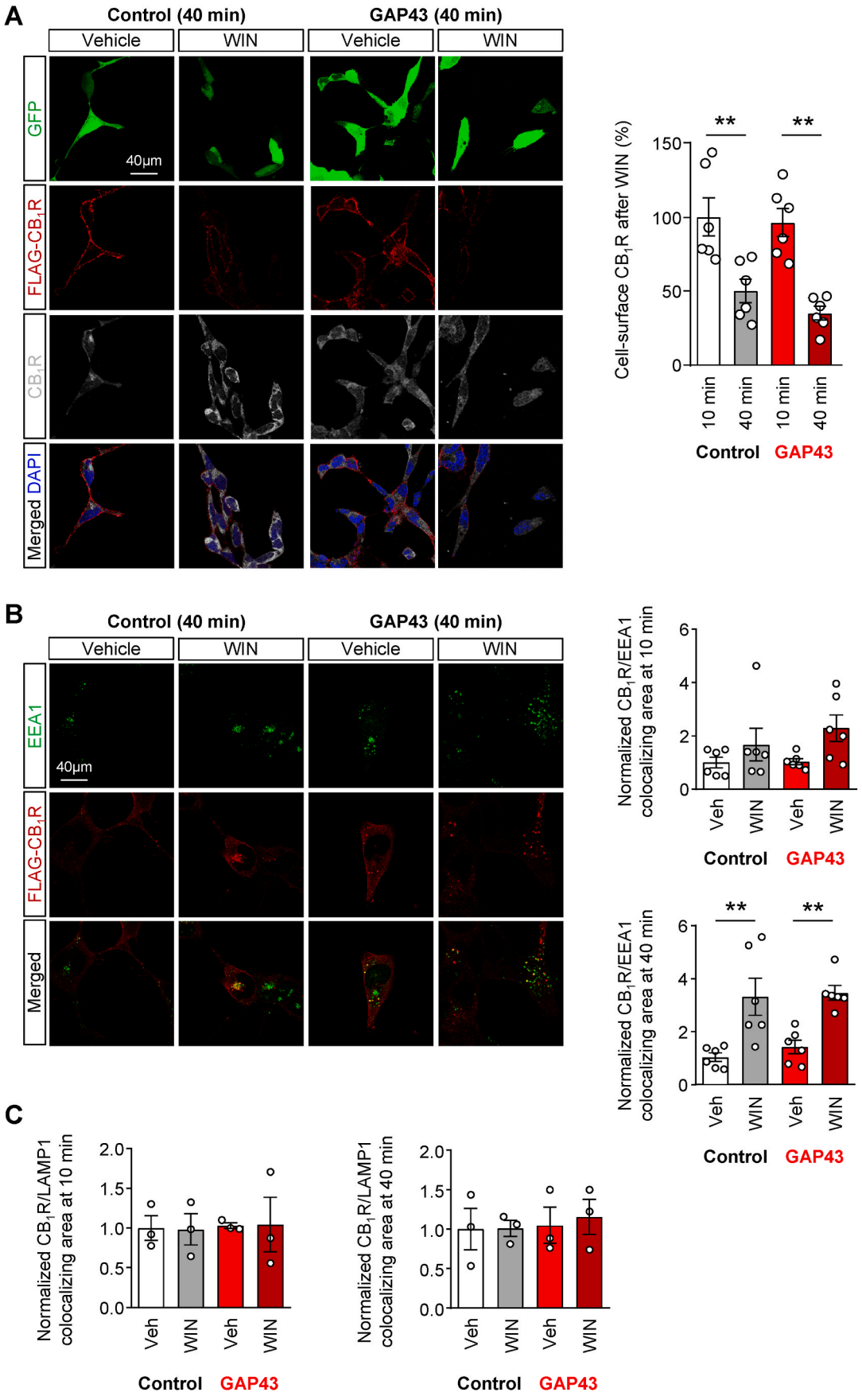

(caption on next page)

Fig. 2. GAP43 does not affect CB_1R internalization and recycling in HEK293T cells. **A.** HEK293T cells expressing an *N*-terminally FLAG-tagged CB_1R, and transfected with a GFP control vector or a GAP43-GFP-encoding vector, were incubated with vehicle or WIN (100 nM, 10 or 40 min). Representative confocal images of GFP control and GAP43-GFP expressing cells upon WIN application (100 nM, 40 min; *left*). Quantification of internalization is expressed as the percentage of surface to total CB_1R, normalized to vehicle (*right*; means ± SEM, n = 6 experiments, $^{**}p < 0.01$ by two-way ANOVA with Tukey's multiple comparison test). **B.** Representative confocal images showing colocalization of CB_1R with early endosome antigen 1 (EEA1) upon WIN application (100 nM, 40 min; *left*). Quantification of CB_1R-EEA1 colocalization after 10 or 40-min WIN challenge (*right*; means ± SEM, n = 6 experiments, $^{**}p < 0.01$ by two-way ANOVA with Tukey's multiple comparison test). **C.** Quantification of CB_1R-lysosomal-associated membrane protein 1 (LAMP1) colocalization after 10 or 40-min WIN challenge (means ± SEM, n = 3 experiments, n. s. by two-way ANOVA with Tukey's multiple comparison test).

0.9837; Fig. 2C), both in the presence and in the absence of GAP43, thus indicating that, at least under these conditions, a negligible WIN-mediated trafficking of CB_1R to lysosomes occurs independently of GAP43 expression levels.

Taken together, these data show that GAP43 does not modulate agonist-evoked CB_1R internalization and subsequent intracellular sorting.

3.3. GAP43 blocks CB_1R-evoked ROCK signalling in HEK293T cells

Given the prominent role of GAP43 in cytoskeletal remodelling and presynaptic plasticity (He et al., 1997; Holahan, 2017), we next aimed to analyse the status of the CB_1R-activated RhoA/ROCK signalling cascade. First, we performed dynamic mass redistribution (DMR) assays, a technique that allows quantifying changes in overall signalling activity triggered by a receptor agonist (Fang et al., 2007), in CB_1R-expressing HEK293T cells (Maroto et al., 2023). Changes in light diffraction were detected at the bottom 150 nm of a cell monolayer. After a baseline period, cells were treated with WIN (100 nM, 0–2000 s) and a specific, saturable response was registered (Fig. 3A). When cells were pre-treated with the ROCK inhibitor Y-27632 (10 μM, 30 min), the WIN-mediated response was partially blocked, thus suggesting that ROCK activation contributes to the global agonist-evoked CB_1R signalling process.

We next conducted Western blot assays to evaluate the effect of GAP43 on this CB_1R-activated cascade (Fig. 3B). WIN (100 nM, 5 min) increased the phosphorylation (activation) of ROCK2, the ROCK isoform that is mainly expressed in the nervous system (Liu et al., 2015), compared to vehicle-treated cells ($F_{(1,\ 28)} = 0.5642$, WIN vs vehicle p = 0.0316). Of note, this effect was abolished upon GAP43 co-expression ($F_{(1,\ 28)} = 0.5642$, WIN vs vehicle p = 0.2628). Similar data were observed for phosphorylated cofilin ($F_{(1,\ 25)} = 1.539$, WIN vs vehicle in control p = 0.0233, WIN vs vehicle in GAP43 p = 0.5899; Fig. 3C), a well-established downstream effector of the ROCK cascade (Liu et al., 2015) (Fig. 3B).

Taken together, these data support that the CB_1R-mediated activation of the ROCK cascade is selectively impaired by GAP43.

3.4. GAP43 blocks CB_1R-evoked ROCK signalling in HEK293T cells by impairing $G\alpha_{q/11}$ protein activation

We have shown above that GAP43 inhibits CB_1R-evoked ROCK signalling but does not affect $G\alpha_{i/o}$ protein coupling to the receptor. Hence, we next aimed at exploring the possible participation of other, non-$G\alpha_{i/o}$ protein subunits. We thus conducted [^{35}S]GTPγS scintillation proximity assays for $G\alpha_{q/11}$, $G\alpha_s$ and $G\alpha_z$, which have been previously shown to associate with CB_1R (Lauckner et al., 2005; Finlay et al., 2017; Garzón et al., 2009), and observed an overt WIN-mediated activation of $G\alpha_{q/11}$ proteins in CB_1R-expressing HEK293T cells ($G\alpha_{q/11}$: $t_{(4)} = 5.081$; p = 0.0071; $G\alpha_s$: $t_{(3)} = 0.2251$; p = 0.8364; $G\alpha_z$: $t_{(3)} = 3.163$; p = 0.0507) that was abolished by GAP43 co-expression ($G\alpha_{q/11}$: $t_{(4)} = 0.5059$; p = 0.6395; $G\alpha_s$: $t_{(4)} = 0.8676$; p = 0.4346; $G\alpha_z$: $t_{(3)} = 1.580$; p = 0.2122; $G\alpha_{q/11}$ control vs $G\alpha_{q/11}$ GAP43 p = 0.0095, $G\alpha_s$ control vs $G\alpha_s$ GAP43 p

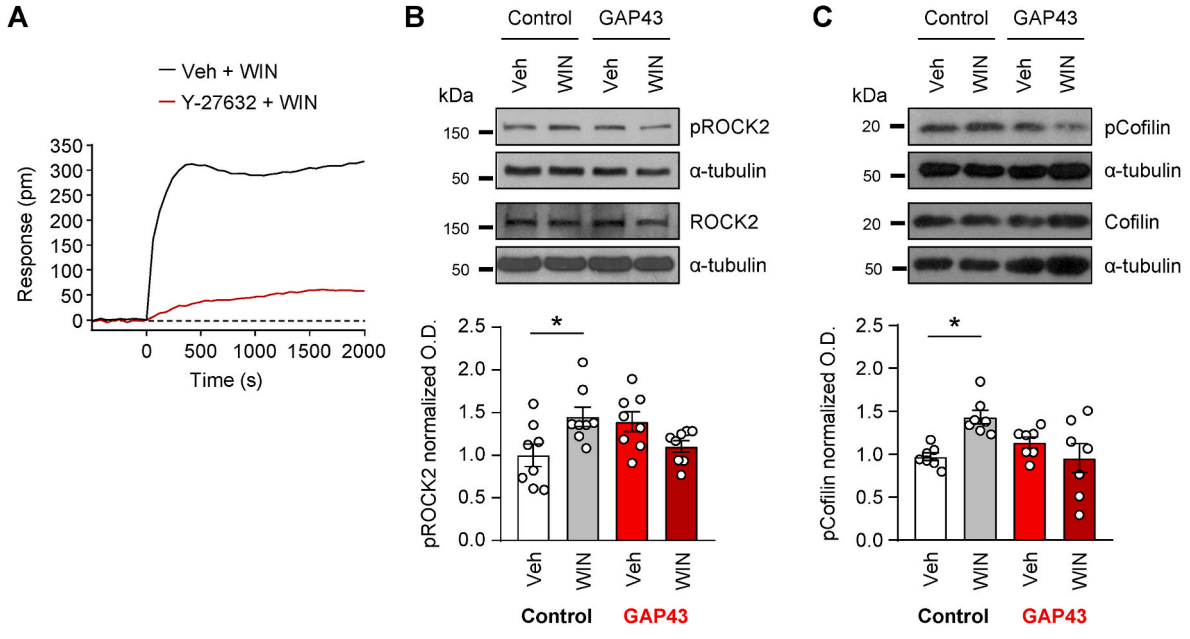

Fig. 3. GAP43 blocks CB_1R-evoked ROCK signaling in HEK293T cells. **A.** DMR assays in HEK293T cells transfected with CB_1R pretreated with vehicle or Y-27632 (10 μM, 30 min) and further challenged with WIN (100 nM). The resulting shifts of reflected light wavelength (in pm) were monitored over time (in s). A representative experiment is shown (n = 3 experiments). **B.** HEK293T cells transfected with CB_1R, and a control vector or a GAP43-encoding vector, were treated with vehicle or WIN (100 nM, 5 min). Representative Western blots and quantification of optical density (O.D.) values of phosphorylated ROCK2 relative to those of the loading control are shown (means ± SEM, n = 8 experiments; $^{*}p < 0.05$ by two-way ANOVA with Tukey's multiple comparison test). **C.** Representative Western blots and quantification of optical density (O.D.) values of phosphorylated cofilin relative to those of the loading control are shown (means ± SEM, n = 7 experiments; $^{*}p < 0.05$ by two-way ANOVA with Tukey's multiple comparison test).

= 0.5701, $G\alpha_z$ control vs $G\alpha_z$ GAP43 p = 0.8234; Fig. 4A). We subsequently performed DMR experiments in cells that were pre-treated with vehicle or the $G\alpha_{q/11}$ inhibitor YM-254890 (1 μM, 30 min). We found an attenuation of the WIN-mediated response by YM-254890 (Fig. 4B), thus supporting that at least part of the global CB_1R signalling activity is due to the coupling of CB_1R to $G\alpha_{q/11}$ proteins.

Then, we pretreated CB_1R-expressing HEK293T cells with vehicle or the $G_{q/11}$ inhibitor YM-254890 (1 μM, 30 min), and subsequently challenged them with vehicle or WIN (100 nM, 5 min), followed by Western blot experiments of ROCK2 and cofilin phosphorylation (Fig. 4C). In control conditions, as observed above, WIN increased the phosphorylation extent of ROCK2 ($F_{(1, 40)} = 9.111$; WIN vs vehicle p = 0.0210) and cofilin ($F_{(1, 20)} = 6.163$; WIN vs vehicle p = 0.0476). Of note, this increase was abolished by YM-254890 (ROCK2: $F_{(1, 40)} = 9.111$; WIN vs vehicle p = 0.6109; cofilin: $F_{(1, 20)} = 6.163$; WIN vs vehicle p = 0.9004), thus mimicking the effect of the ectopic expression of GAP43 and supporting a common mechanism of action.

Taken together, these data indicate that GAP43 reduces agonist-evoked CB_1R signalling in a selective manner by occluding $G_{q/11}$ protein-mediated ROCK pathway activation.

3.5. GAP43 impedes CB_1R-evoked ROCK signalling and neurite collapse in primary hippocampal neurons

Both GAP43 and CB_1R are highly abundant in the central nervous system (Benowitz et al., 1988; Kano et al., 2009; Herkenham et al., 1990) and interact at a subpopulation of hippocampal excitatory boutons (Maroto et al., 2023). Hence, primary cultures of newborn-mouse hippocampal neurons were prepared and analysed after a differentiation period of 7 days *in vitro* (DIV7). A marked overlapping was observed between CB_1R and GAP43, largely at growing neural processes as labelled with βIII-tubulin (Fig. 5A). To study the effect of GAP43 on CB_1R signalling, these DIV7 neuronal cultures were nucleofected with a control vector or a GAP43-encoding vector (Suppl. Fig. 2B) and subsequently treated with vehicle or WIN (100 nM, 5 min). We observed a WIN-mediated increase in phosphorylated ROCK2 by Western blot ($F_{(1, 16)} = 1.574$; p = 0.0416; Fig. 5B) as well as by immunofluorescence assays ($F_{(1, 8)} = 7.838$; p = 0.0247; Fig. 5C). This effect was abrogated in cells overexpressing GAP43 ($F_{(1, 16)} = 1.574$; p = 0.6460, Fig. 5B; $F_{(1, 8)} = 7.838$; p = 0.9940, Fig. 5C), in agreement with the aforementioned observations in HEK293T cells.

Both CB_1R and GAP43 are actively involved in the control of neurite outgrowth (Maccarrone et al., 2014; Holahan, 2017; Strittmatter, 1992). Hence, we aimed to evaluate a possible crosstalk between CB_1R and GAP43 in this process. For this purpose, we measured the length covered by all processes per neuron, as labelled with βIII-tubulin, in our DIV7 primary cultures that had been nucleofected with a control vector or a GAP43-encoding vector. We found a decrease in the mean neurite length upon treatment with WIN (100 nM, 5 min) compared with vehicle-treated neurons, and this effect was abrogated by GAP43 overexpression ($F_{(1, 18)} = 0.3007$; WIN vs vehicle in control p = 0.0210, WIN vs vehicle in GAP43 p = 0.1542; Fig. 5D).

Taken together, these data indicate that GAP43 impedes CB_1R-evoked ROCK signalling in mouse hippocampal neurons, thereby blocking the neurite-growth collapsing effect of the receptor.

3.6. Multiple regions of GAP43 participate in its interaction with CB_1R

We finally aimed to dissect the regions of GAP43 that participate in its interaction with CB_1R. For this purpose, we obtained the HSQC (^1H-^{15}N) spectrum of GAP43 with and without a hCB_1R *C*-terminal stretch (red and blue in Fig. 6A, respectively). The spectrum confirmed the intrinsically disordered nature of GAP43, consistent with the inability of AlphaFold2 software to predict accurately most of its tertiary structure (Suppl. Figs. 3A–C) (Flamm et al., 2016). The addition of the CB_1R *C*-terminal peptide (Suppl. Fig. 3D) did not produce a global rearrangement of the protein, which remained disordered (Fig. 6A). The chemical shift perturbation analysis of GAP43 signals upon peptide

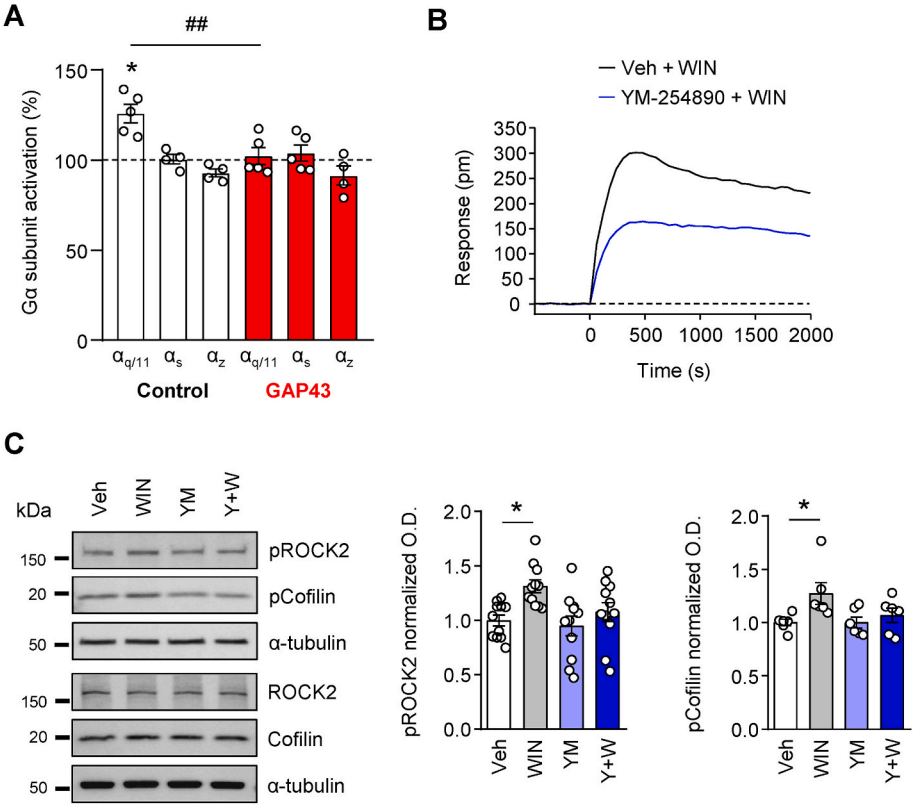

Fig. 4. GAP43 bocks CB_1R-evoked ROCK signaling by impairing $G\alpha_{q/11}$ protein activation in HEK293T cells. **A.** [^{35}S]GTPγS scintillation proximity assays coupled to immunoprecipitation with specific antibodies against non-$G\alpha_{i/o}$ subunits were conducted in membrane homogenates from HEK293T cells transfected with CB_1R, and a control vector or a GAP43-encoding vector. Data are shown as percentage of [^{35}S]GTPγS basal binding values obtained for each specific subunit upon WIN application (means ± SEM, n = 3–5 experiments, 100% indicated with a dashed line, *p < 0.05 from basal by one sample Student's t-test and $^{\#\#}$p < 0.01 from control by two-tailed unpaired Student's t-test). **B.** DMR assays in HEK293T cells transfected with CB_1R pretreated with vehicle or YM-254890 (10 μM, 30 min) and further challenged with WIN (100 nM). The resulting shifts of reflected light wavelength (in pm) were monitored over time (in s). A representative experiment is shown (n = 3 experiments). **C.** HEK293T cells transfected with CB_1R, and a control vector or a GAP43-encoding vector, were treated with vehicle or YM-254890 (YM; 1 μM, 30 min) and then with vehicle or WIN (100 nM, 5 min). Representative Western blots and quantification of optical density (O.D.) values of phosphorylated ROCK2 (means ± SEM, n = 11 experiments; *p < 0.05 by two-way ANOVA with Tukey's multiple comparison test) and cofilin (means ± SEM, n = 6 experiments; *p < 0.05 by two-way ANOVA with Tukey's multiple comparison test) relative to those of the loading control are shown.

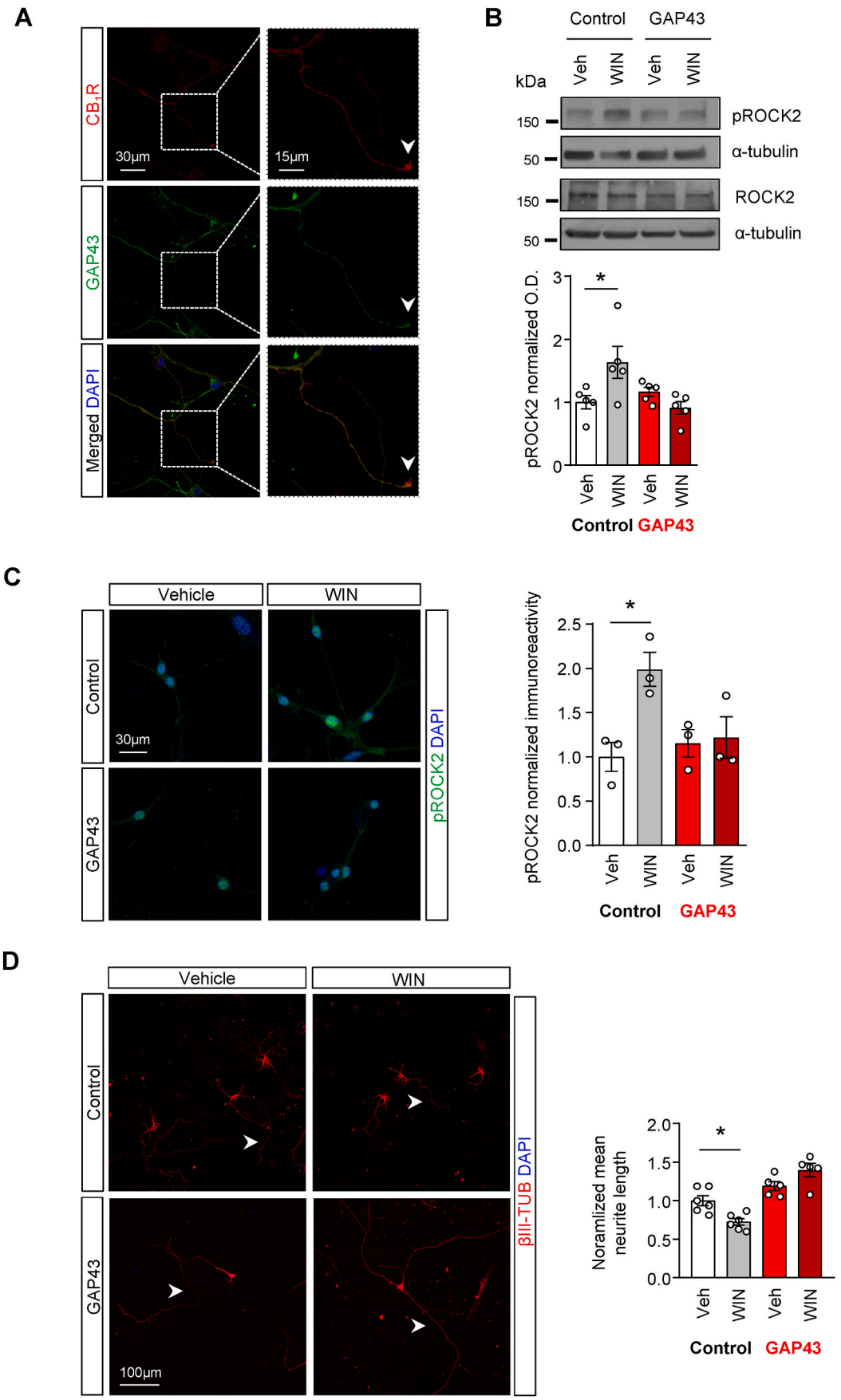

(caption on next page)

Fig. 5. GAP43 impedes CB_1R-evoked ROCK signaling and neurite collapse in primary hippocampal neurons. **A.** Confocal images of mouse hippocampal primary neurons at DIV7 immunolabeled for CB_1R and GAP43. The dotted line depicts the high-magnification inset shown in the right column. The arrowhead points to a sample growth cone where both proteins colocalize. **B**. DIV7 primary neurons nucleofected with a control vector or a GAP43-encoding vector were treated with vehicle or WIN (100 nM, 5 min). Representative Western blots and quantification of optical density (O.D.) values of phosphorylated ROCK2 relative to those of the loading control are shown (means ± SEM, n = 5 experiments, *p < 0.05 by two-way ANOVA with Tukey's multiple comparison test). **C.** Representative confocal images of DIV7 neurons immunolabelled with phosphorylated ROCK2 and β-tubulin III (*left*). Quantification of pROCK2 immunoreactivity (*right*, means ± SEM, n = 3 experiments, *p < 0.05 by two-way ANOVA with Tukey's multiple comparison test). **D**. Representative confocal images of DIV7 neurons immunolabelled with β-tubulin III. Arrowheads point to sample neurites (*left*). Quantification of mean neurite length (*right*, means ± SEM, n = 6–5 experiments, *p < 0.05, **p < 0.01 by two-way ANOVA with Tukey's multiple comparison test).

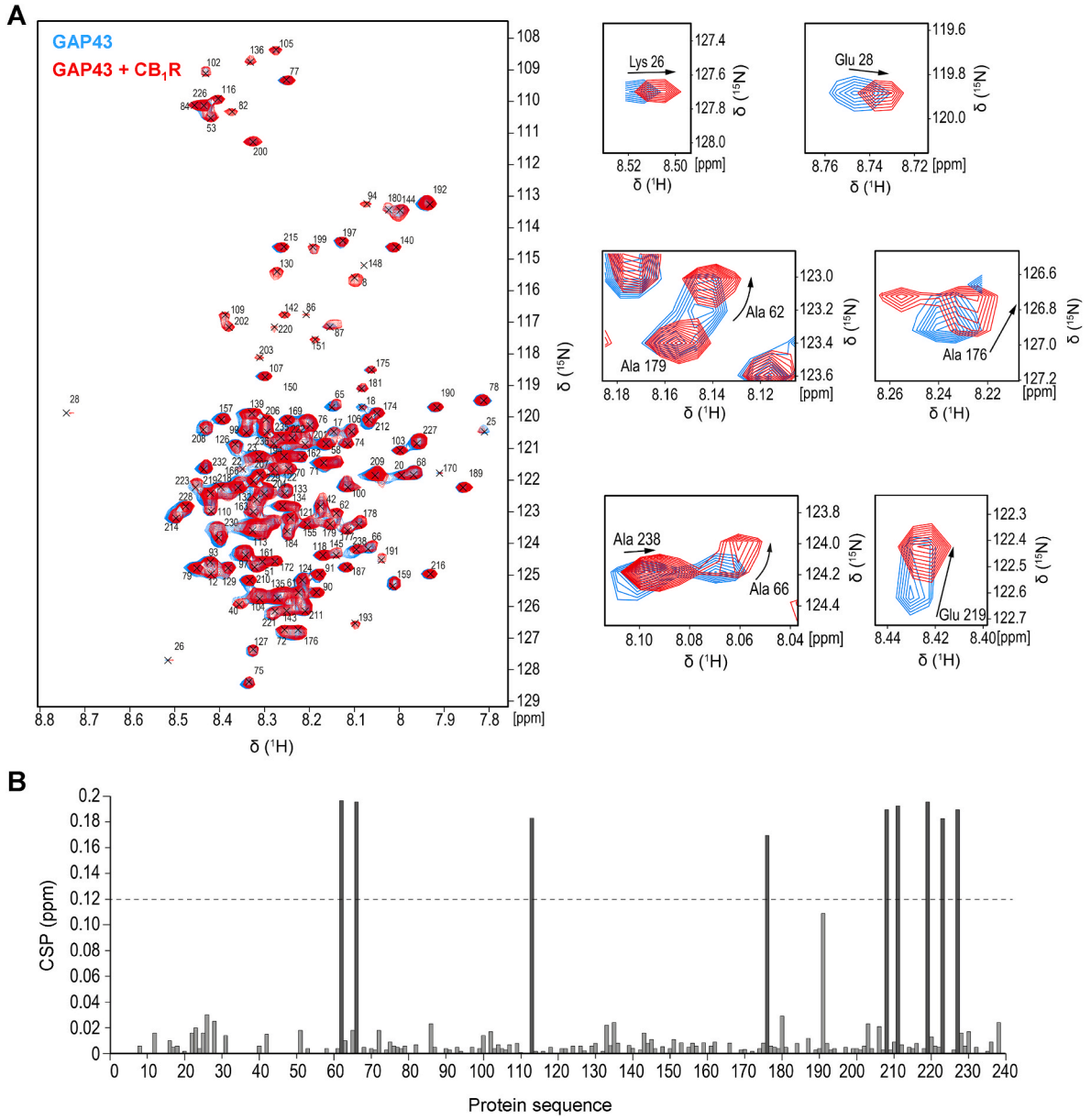

Fig. 6. NMR-based structural analysis of the interaction of GAP43 with the CB_1R *C*-terminal domain. **A.** HSQC (^1H-^{15}N) spectrum of GAP43 with and without a CB_1R *C*-terminal peptide (red and blue, respectively) (*left*). Cross-peak displacement of representative residues are shown (*right*). **B**. Chemical shift perturbation mapping of the GAP43 (^1H-^{15}N) signals upon addition of a hCB_1R *C*-terminal peptide (amino acids 431–458).

addition showed alterations located at both the *N*-terminal and the *C*-terminal domains. However, the residues at the *N*-terminal domain displayed moderate perturbations (most of them with $\Delta\delta \approx 0.02$ ppm) compared to the residues at the *C*-terminal domain (six HNs display $\Delta\delta \approx 0.18$ ppm). (Fig. 6B). Hence, two main regions of GAP43 seemed to be involved in the binding to the CB_1R *C*-terminal domain: a weakly interacting *N*-terminal stretch, involving residues around position 28 and 62–66, and a more strongly interacting *C*-terminal stretch, involving residues mainly around position 220 (Fig. 6B and Suppl. Fig. 3C). These data provide further support to the notion (Maroto et al., 2023) that the inhibitory effect of GAP43 on CB_1R is due to a direct and specific physical interaction of the two proteins.

4. Discussion

Various studies have aimed at discovering proteins that interact with CB_1R and modulate receptor-evoked signalling in a spatiotemporal-selective manner (Leo and Abood, 2021; Oyagawa and Grimsey, 2021; Oliver et al., 2020). We have previously identified a new CB_1R-interacting protein, namely GAP43, long known for its functions in structural plasticity, as an excitatory synapse-specific inhibitor of CB_1R action (Maroto et al., 2023). Here, we went one step ahead by showing that GAP43 modifies CB_1R-mediated signalling activity in a very particular manner. Specifically, our data unveil that the classical CB_1R-associated $G_{i/o}$ protein-coupled signalling cascades, such as cAMP/PKA and ERK, are not affected by GAP43 interaction. In contrast, strikingly, GAP43 selectively modulates an alternative CB_1R-associated $G_{q/11}$ protein-coupled ROCK pathway, thus inducing a delicate bias of the receptor signalling profile.

Previous evidence has shown a functional link between CB_1R and RhoA/ROCK signalling in both neurons (Berghuis et al., 2007; Díaz-Alonso et al., 2016) and non-neural cells (Mai et al., 2015). ROCK belongs to the serine/threonine protein kinase superfamily and is the most relevant downstream effector molecule of the small GTPase Rho, which removes ROCK auto-inhibition. Activated ROCK then phosphorylates its substrates to induce cytoskeletal reorganization. Specifically, LIM kinase is a ROCK downstream substrate that phosphorylates the actin-binding protein cofilin, which then becomes inactivated by phosphorylation, turning incapable of depolymerizing actin chains and of promoting neurite/filopodia extension (Liu et al., 2015). GAP43 is usually considered another actin-binding protein owing to its involvement in the lateral interaction and stabilization of long F-actin filaments (He et al., 1997; Moss et al., 1990). GAP43 interacts as well with other cytoskeleton-associated proteins to favour an actin-polymerization environment (Riederer and Routtenberg, 1999), and can regulate the activity of Rho family members (Aarts et al., 1998). Our findings show that GAP43 abrogates the agonist-evoked CB_1R activation of ROCK and subsequent inactivation of cofilin, which further supports the growth-promoting functions of GAP43 in neurons.

We also show that the pharmacological blockade of $G_{q/11}$ proteins reduces cannabinoid-evoked ROCK and cofilin phosphorylation, thus acting in the same direction as GAP43, which impairs CB_1R-mediated $G_{q/11}$ protein activation. This is the first report supporting that CB_1R couples to a $G_{q/11}$-ROCK signalling axis and that GAP43, conceivably by interacting with the receptor, blocks that process. A previous report showed that a biased agonism of WIN and anandamide at CB_1R triggered Ca^{2+} mobilization from intracellular stores by a preferential activation of $G\alpha_{q/11}$ proteins in HEK293T cells, which might ultimately participate in the control of cytoskeletal dynamics (Lauckner et al., 2005). Likewise, the specific pattern of G protein subunit activation in the mouse brain cortex was found to depend on the cannabinoid agonist used (Diez-Alarcia et al., 2016; Costas-Insua et al., 2021). Regions homologous to the putative CB_1R-*C*-terminal domain α-helix 9 have been suggested to bind $G\alpha_{q/11}$ in rhodopsin (Murakami and Kouyama, 2008) and the bradykinin B2 receptor (Piserchio et al., 2005). According to our data, it would be possible that GAP43 bound to that domain, thus occluding the $G\alpha_{q/11}$-binding site. In fact, we detected by NMR spectroscopy the interaction of GAP43 with a CB_1R *C*-terminal peptide comprising amino acids 431–458, which partially overlaps with the proposed CB_1R-*C*-terminal domain α-helix 9 (amino acids 440–461, Suppl. Fig. 3D (Stadel et al., 2011)). It has also been suggested that the CB_1R-*C*-terminal domain α-helix 9 stabilizes CB_1R at the membrane (Fletcher-Jones et al., 2019), unlike the most distal part of the CB_1R-*C*-terminal domain, that has been largely implicated in receptor internalization processes (Stadel et al., 2011; Hsieh et al., 2002). This aligns with our finding that GAP43 does not affect agonist-evoked CB_1R internalization and endosomal trafficking.

We have previously reported that, like GAP43, the Hsp70 chaperone-family member BiP also interacts with CB_1R and impairs receptor-evoked $G\alpha_{q/11}$ protein activation, although, unlike GAP43, BiP acts in GABAergic neurons rather than in glutamatergic neurons (Costas-Insua et al., 2021; Gómez-Almería et al., 2021). Hence, a set of CB_1R-interacting proteins might operate in a spatiotemporal-selective manner to fine-tune different $CB_1R/G\alpha_{q/11}$-mediated biological processes. In addition, $G\alpha_{12/13}$ protein association to CB_1R, presumably through binding to the intracellular loop 3 of the receptor rather than to its *C*-terminal domain (Inoue et al., 2019), can modulate Rho activity and cytoskeletal architecture in neurons (Dalton et al., 2013; Roland et al., 2014). Moreover, there is evidence supporting that $G\alpha_{12/13}$ and $G\alpha_{q/11}$ can trigger neurite collapse by distinct signaling pathways (Roland et al., 2014; Kranenburg et al., 1999; Katoh et al., 1998). Thus, it is possible that different mechanisms are triggered in neurons compared to HEK293T cells, and we cannot exclude a potential cooperation between $G\alpha_{q/11}$, $G\alpha_{12/13}$ and/or their respective βγ subunits (Dalton et al., 2020) in a neuronal system in which integration of signals from different G proteins determines cytoskeletal dynamics.

On neurobiological grounds, CB_1R was reported to colocalize with GAP43 on axonal cones of extending myelin fibers in the developing rat brain (Gómez et al., 2008). CB_1R activation induces neurite collapse and repulsive growth cone turning, at least *in vitro* (Berghuis et al., 2007; Argaw et al., 2011; Zhou and Song, 2001; Rueda et al., 2002). The molecular mechanism of CB_1R action on the cytoskeletal rearrangements associated to growth cone dynamics was proposed to involve RhoA/ROCK (Berghuis et al., 2007; Roland et al., 2014) among other cascades (He et al., 2005; Bromberg et al., 2008). In fact, the ROCK inhibitor Y-27632 increased the number of long projections in human SH-SY5Y neuroblastoma cells stably expressing CB_1R (Lyons et al., 2020). On the other hand, GAP43, when phosphorylated at the classical PKC-dependent S41 residue, is an archetypical marker of expanding growth cones (Strittmatter et al., 1995). It responds to several extracellular attractive signals to direct the functional behaviour of growth cones (Meiri et al., 1998; Neve et al., 1991). The levels of phosphorylated GAP43 are low in actively retracting branches (Dent and Meiri, 1998), and interfering with GAP43 activation inhibits neurite outgrowth (Benowitz and Routtenberg, 1997). We have previously reported that phosphorylation of the GAP43-S41 residue is required for the interaction with CB_1R and the resulting inhibition of receptor synaptic function (Maroto et al., 2023). It is therefore possible that more extensive changes in the protons surrounding GAP43-S41 could be observed in the NMR spectrum if that residue was phosphorylated in the recombinant protein. As CB_1R and GAP43 show opposed functions in regulating growth cone advance, an inhibitory effect of S41-phosphorylated GAP43 on CB_1R-evoked activation of ROCK signalling fits well in this scenario. CB_1R and GAP43 could likely crosstalk at neuronal processes in response to extracellular signals coming from the niche. Other cytoskeletal proteins such as WAVE1 family members also interact with CB_1R and modulate its function on neurite growth and development (Njoo et al., 2015). Hence, it is conceivable that a subset of the CB_1R interactome is composed by various cytoskeleton-associated proteins that assist the receptor in regulating cytoskeletal dynamics at growth cones and remodelling nerve terminals. Further studies would be required to fully understand the intricate spatiotemporal role of CB_1R-GAP43 complexes at extending neural fibres in the normal and pathological brain.

Funding

This work was supported by the Spanish *Ministerio de Ciencia e Innovación* (MICINN/FEDER; grants PID2021-125118OB-I00 to M.G., PID2020-113938RB-I00 to E.M. and V.C., PID2019-106404RB-I00 to L. U., and PID2019-105237 GB-I00 to A.C.) and the *Generalitat de Catalunya* (grant 2021-SGR-00230 to E.M. and V.C.). I.B.M. and C.C.-I. were supported by contracts from the Spanish *Ministerio de Universidades* (*Formación de Profesorado Universitario* Program, references FPU15/01833 and FPU16/02593, respectively). These funding agencies had no further role in study design, collection, analysis and interpretation of the

data, in the writing of the report, or in the decision to submit the paper for publication.

CRediT authorship contribution statement

Irene B. Maroto: Conceptualization, Data curation, Formal analysis, Investigation, Methodology, Resources, Software, Supervision, Validation, Visualization, Writing – original draft, Writing – review & editing. **Estefanía Moreno:** Data curation, Formal analysis, Investigation, Methodology, Resources, Software, Validation, Visualization, Writing – review & editing. **Carlos Costas-Insua:** Conceptualization, Formal analysis, Investigation, Methodology, Resources, Validation, Visualization, Writing – review & editing. **Javier Merino-Gracia:** Formal analysis, Investigation, Methodology, Software, Validation, Visualization, Writing – review & editing. **Rebeca Diez-Alarcia:** Formal analysis, Investigation, Methodology, Software, Writing – review & editing. **Alicia Álvaro-Blázquez:** Investigation, Methodology, Software, Writing – review & editing. **Ángeles Canales:** Funding acquisition, Methodology, Resources, Supervision, Writing – review & editing. **Enric I. Canela:** Funding acquisition, Methodology, Resources, Supervision, Writing – review & editing. **Vicent Casadó:** Funding acquisition, Methodology, Resources, Supervision, Writing – review & editing. **Leyre Urigüen:** Data curation, Formal analysis, Funding acquisition, Methodology, Resources, Software, Supervision, Validation, Writing – review & editing. **Ignacio Rodríguez-Crespo:** Conceptualization, Data curation, Formal analysis, Methodology, Resources, Software, Supervision, Validation, Writing – review & editing. **Manuel Guzmán:** Conceptualization, Data curation, Formal analysis, Funding acquisition, Methodology, Project administration, Supervision, Validation, Visualization, Writing – original draft, Writing – review & editing.

Declaration of competing interest

The authors declare the following financial interests/personal relationships which may be considered as potential competing interests: Manuel Guzmán reports financial support was provided by Spain Ministry of Science and Innovation. Vicent Casadó reports financial support was provided by Spain Ministry of Science and Innovation. Ángeles Canales reports financial support was provided by Spain Ministry of Science and Innovation. Leyre Urigüen reports financial support was provided by Spain Ministry of Science and Innovation. Estefanía Moreno reports financial support was provided by Generalitat de Catalunya Ministry of Research and Universities.

Data availability

Data will be made available on request.

Acknowledgements

We are indebted to Andrea Macías-Camero, Beatriz Monforte-Martínez and the personnel of the microscope imaging centre of Complutense University of Madrid for their expert technical assistance.

Appendix A. Supplementary data

Supplementary data to this article can be found online at https://doi.org/10.1016/j.neuropharm.2023.109712.

References

Aarts, L.H.J., Schrama, L.H., Hage, W.J., et al., 1998. B-50/GAP-43-induced formation of filopodia depends on Rho-GTPase. Mol. Biol. Cell 9, 1279–1292. https://doi.org/10.1091/mbc.9.6.1279.

Anavi-Goffer, S., Fleischer, D., Hurst, D.P., et al., 2007. Helix 8 Leu in the CB1 cannabinoid receptor contributes to selective signal transduction mechanisms. J. Biol. Chem. 282, 25100–25113. https://doi.org/10.1074/jbc.M703388200.

Argaw, A., Duff, G., Zabouri, N., et al., 2011. Concerted action of CB_1 cannabinoid receptor and deleted in colorectal cancer in axon guidance. J. Neurosci. 31, 1489–1499. https://doi.org/10.1523/JNEUROSCI.4134-09.2011.

Benowitz, L.I., Routtenberg, A., 1997. GAP-43: an intrinsic determinant of neuronal development and plasticity. Trends Neurosci. 20, 84–91. https://doi.org/10.1016/S0166-2236(96)10072-2.

Benowitz, L.I., Apostolides, P.J., Perrone-Bizzozero, N., et al., 1988. Anatomical distribution of the growth-associated protein GAP-43/B-50 in the adult rat brain. J. Neurosci. 8, 339–352. https://doi.org/10.1523/JNEUROSCI.08-01-00339.1988.

Berghuis, P., Rajnicek, A.M., Morozov, Y.M., et al., 2007. Hardwiring the brain: endocannabinoids shape neuronal connectivity. Science 316, 1212–1216. https://doi.org/10.1126/science.1137406.

Blázquez, C., Chiarlone, A., Sagredo, O., et al., 2011. Loss of striatal type 1 cannabinoid receptors is a key pathogenic factor in Huntington's disease. Brain 134, 119–136. https://doi.org/10.1093/brain/awq278.

Bromberg, K.D., Ma'ayan, A., Neves, S.R., Iyengar, R., 2008. Design logic of a cannabinoid receptor signaling network that triggers neurite outgrowth. Science 320, 903–909. https://doi.org/10.1126/science.1152662.

Burford, N.T., Tolbert, L.M., Sadee, W., 1998. Specific G protein activation and μ-opioid receptor internalization caused by morphine, DAMGO and endomorphin I. Eur. J. Pharmacol. 342, 123–126. https://doi.org/10.1016/S0014-2999(97)01556-2.

Costas-Insua, C., Moreno, E., Maroto, I.B., et al., 2021. Identification of BiP as a CB_1 receptor-interacting protein that fine-tunes cannabinoid signaling in the mouse brain. J. Neurosci. 41, 7924–7941. https://doi.org/10.1523/JNEUROSCI.0821-21.2021.

Dalton, G.D., Peterson, L.J., Howlett, A.C., 2013. CB_1 cannabinoid receptors promote maximal FAK catalytic activity by stimulating cooperative signaling between receptor tyrosine kinases and integrins in neuronal cells. Cell. Signal. 25, 1665–1677. https://doi.org/10.1016/j.cellsig.2013.03.020.

Dalton, G.D., Carney, S.T., Marshburn, J.D., et al., 2020. CB_1 Cannabinoid receptors stimulate Gβγ-GRK2-mediated FAK phosphorylation at tyrosine 925 to regulate ERK activation involving neuronal focal adhesions. Front. Cell. Neurosci. 14, 176. https://doi.org/10.3389/fncel.2020.00176.

Dent, E.W., Meiri, K.F., 1998. Distribution of phosphorylated GAP-43 (neuromodulin) in growth cones directly reflects growth cone behavior. J. Neurobiol. 35, 287–299. https://doi.org/10.1002/(SICI)1097-4695(19980605)35:3<287::AID-NEU6>3.0.CO;2-V.

Díaz-Alonso, J., de Salas-Quiroga, A., Paraíso-Luna, J., et al., 2016. Loss of cannabinoid CB_1 receptors induces cortical migration malformations and increases seizure susceptibility. Cerebr. Cortex 27, 5303–5317. https://doi.org/10.1093/cercor/bhw309.

Diez-Alarcia, R., Ibarra-Lecue, I., Lopez-Cardona, Á.P., et al., 2016. Biased agonism of three different cannabinoid receptor agonists in mouse brain cortex. Front. Pharmacol. 7, 415. https://doi.org/10.3389/fphar.2016.00415.

Fang, Y., Li, G., Ferrie, A.M., 2007. Non-invasive optical biosensor for assaying endogenous G protein-coupled receptors in adherent cells. J. Pharmacol. Toxicol. Methods 55, 314–322. https://doi.org/10.1016/j.vascn.2006.11.001.

Finlay, D.B., Cawston, E.E., Grimsey, N.L., et al., 2017. Gαs signalling of the CB_1 receptor and the influence of receptor number. Br. J. Pharmacol. 174, 2545–2562. https://doi.org/10.1111/bph.13866.

Flamm, A.G., Żerko, S., Zawadzka-Kazimierczuk, A., et al., 2016. 1H, 15N, 13C resonance assignment of human GAP-43. Biomol NMR Assign 10, 171–174. https://doi.org/10.1007/s12104-015-9660-9.

Fletcher-Jones, A., Hildick, K.L., Evans, A.J., et al., 2019. The C-terminal helix 9 motif in rat cannabinoid receptor type 1 regulates axonal trafficking and surface expression. Elife 8, e44252. https://doi.org/10.7554/eLife.44252.

Fletcher-Jones, A., Hildick, K.L., Evans, A.J., et al., 2020. Protein interactors and trafficking pathways that regulate the cannabinoid type 1 receptor (CB1R). Front. Mol. Neurosci. 13, 108. https://doi.org/10.3389/fnmol.2020.00108.

Garzón, J., de la Torre-Madrid, E., Rodríguez-Muñoz, M., et al., 2009. Gz mediates the long-lasting desensitization of brain CB_1 receptors and is essential for cross-tolerance with morphine. Mol. Pain 5, 11. https://doi.org/10.1186/1744-8069-5-11.

Gómez, M., Hernández, M.L., Pazos, M.R., et al., 2008. Colocalization of CB_1 receptors with L1 and GAP-43 in forebrain white matter regions during fetal rat brain development: evidence for a role of these receptors in axonal growth and guidance. Neuroscience 153, 687–699. https://doi.org/10.1016/j.neuroscience.2008.02.038.

Gómez-Almería, M., Burgaz, S., Costas-Insua, C., et al., 2021. Bip heterozigosity aggravates pathological deterioration in experimental amyotrophic lateral sclerosis. Int. J. Mol. Sci. 22, 12533 https://doi.org/10.3390/ijms222212533.

Han, M.H., Jiao, S., Jia, J.M., et al., 2013. The novel caspase-3 substrate Gap43 is involved in AMPA receptor endocytosis and long-term depression. Mol. Cell. Proteomics 12, 3719–3731. https://doi.org/10.1074/mcp.M113.030676.

He, Q., Dent, E.W., Meiri, K.F., 1997. Modulation of actin filament behavior by GAP-43 (neuromodulin) is dependent on the phosphorylation status of serine 41, the protein kinase C site. J. Neurosci. 17, 3515–3524. https://doi.org/10.1523/JNEUROSCI.17-10-03515.1997.

He, J.C., Gomes, I., Nguyen, T., et al., 2005. The $G_{\alpha o/i}$-coupled cannabinoid receptor-mediated neurite outgrowth involves Rap regulation of Src and Stat3. J. Biol. Chem. 280, 33426–33434. https://doi.org/10.1074/jbc.M502812200.

Herkenham, M., Lynn, A.B., Little, M.D., et al., 1990. Cannabinoid receptor localization in brain. Proc. Natl. Acad. Sci. U.S.A. 87, 1932–1936. https://doi.org/10.1073/pnas.87.5.1932.

Holahan, M.R., 2017. A shift from a pivotal to supporting role for the growth-associated protein (GAP-43) in the coordination of axonal structural and functional plasticity. Front. Cell. Neurosci. 11, 1–19. https://doi.org/10.3389/fncel.2017.00266.

Howlett, A.C., Abood, M.E., 2017. CB_1 and CB_2 receptor pharmacology. In: Advances in Pharmacology, pp. 169–206.
Howlett, A.C., Qualy, J.M., Khachatrian, L.L., 1986. Involvement of Gi in the inhibition of adenylate cyclase by cannabimimetic drugs. Mol. Pharmacol. 29, 307–313.
Hsieh, C., Brown, S., Derleth, C., Mackie, K., 2002. Internalization and recycling of the CB_1 cannabinoid receptor. J. Neurochem. 73, 493–501. https://doi.org/10.1046/j.1471-4159.1999.0730493.x.
Inoue, A., Raimondi, F., Kadji, F.M.N., et al., 2019. Illuminating G-protein-coupling selectivity of GPCRs. Cell 177, 1933–1947. https://doi.org/10.1016/j.cell.2019.04.044.
Kano, M., Ohno-Shosaku, T., Hashimotodani, Y., et al., 2009. Endocannabinoid-mediated control of synaptic transmission. Physiol. Rev. 89, 309–380. https://doi.org/10.1152/physrev.00019.2008.
Katoh, H., Aoki, J., Yamaguchi, Y., et al., 1998. Constitutively active Gα12, Gα13, and Gαq induce rho-dependent neurite retraction through different signaling pathways. J. Biol. Chem. 273, 28700–28707. https://doi.org/10.1074/jbc.273.44.28700.
Katona, I., Freund, T.F., 2008. Endocannabinoid signaling as a synaptic circuit breaker in neurological disease. Nat. Med. 14, 923–930. https://doi.org/10.1038/nm.f.1869.
Kranenburg, O., Poland, M., Van Horck, F.P.G., et al., 1999. Activation of RhoA by lysophosphatidic acid and $G\alpha_{12/13}$ subunits in neuronal cells: induction of neurite retraction. Mol. Biol. Cell 10, 1851–1857. https://doi.org/10.1091/mbc.10.6.1851.
Lauckner, J.E., Hille, B., Mackie, K., 2005. The cannabinoid agonist WIN55,212-2 increases intracellular calcium via CB_1 receptor coupling to $G_{q/11}$ G proteins. Proc. Natl. Acad. Sci. U.S.A. 102, 19144–19149. https://doi.org/10.1073/pnas.0509588102.
Leo, L.M., Abood, M.E., 2021. CB1 cannabinoid receptor signaling and biased signaling. Molecules 26, 5413. https://doi.org/10.3390/molecules26175413.
Liu, J., Gao, H., Wang, X., 2015. The role of the Rho/ROCK signaling pathway in inhibiting axonal regeneration in the central nervous system. Neural Regen. Res. 10, 1892. https://doi.org/10.4103/1673-5374.170325.
Lyons, E.L., Leone-Kabler, S., Kovach, A.L., et al., 2020. Cannabinoid receptor subtype influence on neuritogenesis in human SH-SY5Y cells. Mol. Cell. Neurosci. 109, 103566 https://doi.org/10.1016/j.mcn.2020.103566.
Maccarrone, M., Guzmán, M., Mackie, K., et al., 2014. Programming of neural cells by (endo)cannabinoids: from physiological rules to emerging therapies. Nat. Rev. Neurosci. 15, 786–801. https://doi.org/10.1038/nrn3846.
Mai, P., Tian, L., Yang, L., et al., 2015. Cannabinoid receptor 1 but not 2 mediates macrophage phagocytosis by $G_{\alpha i/o}$/RhoA/ROCK signaling pathway. J. Cell. Physiol. 230, 1640–1650. https://doi.org/10.1002/jcp.24911.
Maroto, I.B., Costas-Insua, C., Berthoux, C., et al., 2023. Control of a hippocampal recurrent excitatory circuit by cannabinoid receptor-interacting protein Gap43. Nat. Commun. 14, 2303. https://doi.org/10.1038/s41467-023-38026-2.
Martini, L., Waldhoer, M., Pusch, M., et al., 2007. Ligand-induced down-regulation of the cannabinoid 1 receptor is mediated by the G-protein-coupled receptor-associated sorting protein GASP1. Faseb. J. 21, 802–811. https://doi.org/10.1096/fj.06-7132com.
Meiri, K.F., Saffell, J.L., Walsh, F.S., Doherty, P., 1998. Neurite outgrowth stimulated by neural cell adhesion molecules requires growth-associated protein-43 (GAP-43) function and is associated with GAP-43 phosphorylation in growth cones. J. Neurosci. 18, 10429–10437. https://doi.org/10.1523/JNEUROSCI.18-24-10429.1998.
Moreno, E., Andradas, C., Medrano, M., et al., 2014. Targeting CB_2-GPR55 receptor heteromers modulates cancer cell signaling. J. Biol. Chem. 289, 21960–21972. https://doi.org/10.1074/jbc.M114.561761.
Moss, D.J., Fernyhough, P., Chapman, K., et al., 1990. Chicken growth-associated protein GAP-43 is tightly bound to the actin-rich neuronal membrane skeleton. J. Neurochem. 54, 729–736. https://doi.org/10.1111/j.1471-4159.1990.tb02312.x.
Murakami, M., Kouyama, T., 2008. Crystal structure of squid rhodopsin. Nature 453, 363–367. https://doi.org/10.1038/nature06925.
Mureddu, L.G., Ragan, T.J., Brooksbank, E.J., Vuister, G.W., 2020. CcpNmr AnalysisScreen, a new software programme with dedicated automated analysis tools for fragment-based drug discovery by NMR. J. Biomol. NMR 74, 565–577. https://doi.org/10.1007/s10858-020-00321-1.
Neve, R.L., Ivins, K.J., Benowitz, L.I., et al., 1991. Molecular analysis of the function of the neuronal growth-associated protein GAP-43 by genetic intervention. Mol. Neurobiol. 5, 131–141. https://doi.org/10.1007/BF02935542.
Njoo, C., Agarwal, N., Lutz, B., Kuner, R., 2015. The cannabinoid receptor CB_1 interacts with the WAVE1 complex and plays a role in actin dynamics and structural plasticity in neurons. PLoS Biol. 13, e1002286 https://doi.org/10.1371/journal.pbio.1002286.
Nogueras-Ortiz, C., Yudowski, G.A., 2016. The multiple waves of cannabinoid 1 receptor signaling. Mol. Pharmacol. 90, 620–626. https://doi.org/10.1124/mol.116.104539.
Oliver, E.E., Hughes, E.K., Puckett, M.K., et al., 2020. Cannabinoid receptor interacting protein 1a (CRIP1a) in health and disease. Biomolecules 10, 1609. https://doi.org/10.3390/biom10121609.
Oyagawa, C.R.M., Grimsey, N.L., 2021. Cannabinoid receptor CB_1 and CB_2 interacting proteins: techniques, progress and perspectives. Methods Cell Biol. 166, 83–132. https://doi.org/10.1016/bs.mcb.2021.06.011.
Pertwee, R.G., Howlett, A.C., Abood, M.E., et al., 2010. International union of basic and clinical pharmacology. LXXIX. Cannabinoid receptors and their ligands: beyond CB_1 and CB_2. Pharmacol. Rev. 62, 588–631. https://doi.org/10.1124/pr.110.003004.
Piomelli, D., 2003. The molecular logic of endocannabinoid signalling. Nat. Rev. Neurosci. 4, 873–884. https://doi.org/10.1038/nrn1247.
Piserchio, A., Zelesky, V., Yu, J., et al., 2005. Bradykinin B2 receptor signaling: structural and functional characterization of the C-terminus. Biopolymers 80, 367–373. https://doi.org/10.1002/bip.20220.
Riederer, B.M., Routtenberg, A., 1999. Can GAP-43 interact with brain spectrin? Brain Res. Mol. Brain Res. 71, 345–348. https://doi.org/10.1016/s0169-328x(99)00179-5.
Roland, A.B., Ricobaraza, A., Carrel, D., et al., 2014. Cannabinoid-induced actomyosin contractility shapes neuronal morphology and growth. Elife 3, e03159. https://doi.org/10.7554/eLife.03159.
Rueda, D., Navarro, B., Martinez-Serrano, A., et al., 2002. The endocannabinoid anandamide inhibits neuronal progenitor cell differentiation through attenuation of the Rap1/B-Raf/ERK pathway. J. Biol. Chem. 277, 46645–46650. https://doi.org/10.1074/jbc.M206590200.
Skinner, S.P., Fogh, R.H., Boucher, W., et al., 2016. CcpNmr AnalysisAssign: a flexible platform for integrated NMR analysis. J. Biomol. NMR 66, 111–124. https://doi.org/10.1007/s10858-016-0060-y.
Stadel, R., Ahn, K.H., Kendall, D.A., 2011. The cannabinoid type-1 receptor carboxyl-terminus, more than just a tail. J. Neurochem. 117, 1–18. https://doi.org/10.1111/j.1471-4159.2011.07186.x.
Strittmatter, S.M., 1992. GAP-43 as a modulator of G protein transduction in the growth cone. Perspect. Dev. Neurobiol. 1, 13–19.
Strittmatter, S.M., Fankhauser, C., Huang, P.L., et al., 1995. Neuronal pathfinding is abnormal in mice lacking the neuronal growth cone protein GAP-43. Cell 80, 445–452. https://doi.org/10.1016/0092-8674(95)90495-6.
Zhou, D., Song, Z.H., 2001. CB1 cannabinoid receptor-mediated neurite remodeling in mouse neuroblastoma N1E-115 cells. J. Neurosci. Res. 65, 346–353. https://doi.org/10.1002/jnr.1160.
Zhuang, H., Matsunami, H., 2008. Evaluating cell-surface expression and measuring activation of mammalian odorant receptors in heterologous cells. Nat. Protoc. 3, 1402–1413. https://doi.org/10.1038/nprot.2008.120.